A nanobody against the VWF A3 domain detects ADAMTS13-induced proteolysis in congenital and acquired VWD

Claire Kizlik-Masson, Ivan Peyron, Stéphane Gangnard, Gaelle Le Goff, Solen Lenoir, Sandra Damodaran, Marie Clavel, Stéphanie Roullet, Véronique Regnault, Antoine Rauch, et al.

A nanobody against the von Wilebrand factor A3-domain detects ADAMTS13-induced proteolysis in congenital & acquired VWD

Claire Kizlik-Masson[1,*], Ivan Peyron[1,*], Stéphane Gangnard[1], Gaelle Le Goff[2], Solen M Lenoir[2], Sandra Damodaran[2], Marie Clavel[3], Stéphanie Roullet[1], Véronique Regnault[4], Antoine Rauch[5], Flavien Vincent[5], Emmanuelle Jeanpierre[5], Annabelle Dupont[5], Catherine Ternisien[6], Thibault Donnet[2], Olivier D. Christophe[1], Eric van Belle[5], Cécile V. Denis[1], Caterina Casari[1], Sophie Susen[5,6], Peter J. Lenting[1]

[1]Laboratory for Hemostasis, Inflammation & Thrombosis, Unité Mixed de Recherche 1176, Institut National de la Santé et de la Recherche Médicale, Université Paris-Saclay, 94276 Le Kremlin-Bicêtre, France

[2]Diagnostica Stago, Unités de recherche & développement, Gennevilliers, France

[3]Inovarion, Paris, France

[4]Université de Lorraine, Laboratory for Acute and Chronic Cardiovascular Deficiency (DCAC), Institut National de la Santé et de la Recherche Médicale Unité 1116, Nancy, France

[5]Université de Lille, Centre Hospitalier Universitaire Lille, Institut Pasteur de Lille, Institut National de la Santé et de la Recherche Médicale Unité 1011, Lille, France

[6]French Reference Center for von Willebrand disease (CRMW), Lille, France

Authorship Contributions: CKM, IP, SG, GLF, SML, SD, MC, SR, TD, CC and PJL performed experiments and analyzed data; VR, AR, FV, EJ, AD, CT and EvB provided patient samples; SS, ODC, PJL, CVD designed and supervised the study. All authors contributed to the interpretation of the data. PJL wrote the first draft of the manuscript, and all authors contributed to the editing of the final manuscript.

*CKM and IP contributed equally to this manuscript.

Correspondence:

Peter J. Lenting, Inserm U1176, 80 rue du Général Leclerc, 94270 Le Kremlin-Bicetre, France

Tel: +331-49595600; Fax: +33146719472; Email: peter.lenting@inserm.fr

Running title: An anti-A3 domain nanobody detecting intact-VWF

Data sharing statement: Data are available upon reasonable request to the corresponding author

Word count: 3972; **Abstract:** 250; **References:** 36; **Figures:** 6

Key points

Nanobody KB-VWF-D3.1 binds to the collagen-binding site in the VWF A3-domain, and loses its binding upon proteolysis of VWF by ADAMTS13

KB-VWF-D3.1 identified VWF degradation in VWD-patients, which correlated with a loss of larger VWF-multimers

Abstract

Von Willebrand factor (VWF) is a multimeric protein, the size of which is regulated via ADAMTS13-mediated proteolysis within the A2-domain. We aimed to isolate nanobodies distinguishing between proteolyzed and non-proteolyzed VWF, leading to the identification of a nanobody (designated KB-VWF-D3.1) targeting the A3-domain, the epitope of which overlaps the collagen-binding site. While KB-VWF-D3.1 binds with similar efficiency to dimeric and multimeric derivatives of VWF, binding to VWF was lost upon proteolysis by ADAMTS13, suggesting that proteolysis in the A2-domain modulates exposure of its epitope in the A3-domain. We therefore used KB-VWF-D3.1 to monitor VWF degradation in plasma samples. Spiking experiments showed that a loss of 10% intact-VWF could be detected using this nanobody. By comparing plasma from volunteers to that of congenital VWD-patients, intact-VWF levels were significantly reduced for all VWD-types, and most severely in VWD-type 2A-group 2 in which mutations promote ADAMTS13-mediated proteolysis. Unexpectedly, we also observed increased proteolysis in some patients with VWD-type 1 and VWD-type 2M. A significant correlation ($r=0.51$, $p<0.0001$) between the relative amount of high molecular weight-multimers and levels of intact-VWF was observed. Reduced levels of intact-VWF were further found in plasmas from patients with severe aortic stenosis and patients receiving mechanical circulatory support.

KB-VWF-D3.1 is thus a nanobody that detects changes in the exposure of its epitope within the collagen-binding site of the A3-domain. In view of its unique characteristics, it has the potential to be used as a diagnostic tool to investigate whether a loss of larger multimers is due to ADAMTS13-mediated proteolysis.

Introduction

Von Willebrand factor is a multimeric protein, the extent of which regulates its interaction with platelets. Multimerization of VWF occurs during its synthesis in megakaryocytes or endothelial cells.[1,2] In this process, two VWF subunits (with the domain structure: D1-D2-D'-D3-A1-A2-A3-D4-C1-C2-C3-C4-C5-C6-CK) are first covalently linked via disulfide bridging between two C-terminal CK-domains. These pro-dimers are then processed into multimers via N-terminal coupling of the D'-D3 regions, with the D1-D2 portion (also known as VWF propeptide) being eliminated during this event. The multimer size in endothelial cells is highly variable and varies from dimers to ultra-large multimers with >40 subunits. Upon secretion, VWF multimers are susceptible to regulated proteolysis by ADAMTS13, a metalloprotease that cleaves VWF in its A2-domain at the Tyr^{1605}-Met^{1606} peptide bond.[3] Importantly, proteolysis occurs only upon decryption of the cleavage site, which normally lies buried within the A2-domain.[4]

There are several occurrences that allow for the exposure of the ADAMTS13-cleavage site. First, multiple VWF multimers assemble at the endothelial surface upon stimulated secretion, forming elongated fibers that are proteolyzed by ADAMTS13.[5-7] Second, VWF unfolds during circulation under conditions of increased shear stress or disturbed blood flow.[8] When disturbed blood flow is exaggerated, like in patients having severe aortic stenosis or those who require mechanical circulatory support, excessive VWF degradation may occur, which is then referred to as acquired von Willebrand syndrome (AVWS).[9-11] Third, mutations within VWF may provoke exposure of the ADAMTS13 proteolytic site, and such mutations are most frequently found in von Willebrand disease (VWD)-type 2A-group 2 and VWD-type 2B.[12,13]

Excessive proteolysis of VWF is associated with an increased loss of high molecular weight (HMW)-multimers, which results in reduced platelet binding and reduced collagen binding, thereby increasing the risk of bleeding.[9] The classic approach to visualize the extent of VWF degradation is to analyze the multimeric pattern using SDS-agarose electrophoresis.[14] This approach is laborious, non-standardized and requires 24-72h, dependent on the method that is used. Alternatively, collagen- or platelet-binding assays are used[15], which are less specific in that they do not distinguish between impaired multimerization and excessive degradation. Finally, Kato and colleagues described a monoclonal antibody that binds to the newly formed C-terminal end in the A2-domain (residues Asp^{1596}-Tyr^{1605}). This antibody was successfully used to measure ADAMTS13 activity in patients with thrombotic thrombocytopenic purpura.[16] In addition, we and others used this antibody to monitor VWF proteolysis in patients.[17,18] However, while using an antibody targeting residues Asp^{1596}-Tyr^{1605}, we noticed that this antibody was unable to detect degradation, for instance in samples from patients with non-severe aortic stenosis or with congenital VWD-type 1 or 2M.

In the present study, we have developed a nanobody (designated KB-VWF-D3.1) that distinguishes between intact and ADAMTS13-cleaved VWF. Interestingly, this nanobody binds to the A3-domain, showing that proteolysis within the A2-domain modifies the exposure of the nanobody's epitope in the adjacent A3-domain. This nanobody proved sensitive to detect degradation in plasma from patients with AVWS and congenital VWD, including types 1 and 2M.

Materials & methods

An extensive description of the experimental procedures can be found in the Supplementary methods (available on the *Blood* website).

Ethics statement:

All volunteers and patients provided informed written consent according to the Declaration of Helsinki. Patients with VWD were selected from the French cohort multicentric database of VWD (Centre Reference Maladie Willebrand).[19] The database and biobank of this cohort are declared to and approved by the French data protection authority (CNIL-1245379/DEC-19252, CODECOH-DC-2008-642). Patients with severe aortic stenosis (WITAVI-trial, NCT02628509) and patients receiving extracorporal mechanical oxidation (ECMO; WITECMO-H-trial; NCT03070912) were included in the study. All protocols were approved by the local review and ethics committees.

Isolation of anti-VWF nanobodies

A synthetic nanobody-encoding phage-library[20] was used to isolate anti-VWF nanobodies. The library ($3x10^9$ clones) was incubated with streptavidin-coated beads loaded with biotinylated rVWF. Unbound phages were then incubated with beads loaded with biotinylated degraded-VWF. Three rounds of phage-display were performed, with the depletion step being repeated every round. Twelve unique sequences were obtained via this procedure (Fig. 1A).

Analysis of VWF binding to nanobodies

Wells coated with nanobody KB-VWF-D3.1 or KB-VWF-1.1 (both 5 μg/ml) were incubated with purified rVWF (0-0.5 μg/ml). Bound VWF was probed using polyclonal anti-VWF antibodies and detected via hydrolysis of 3,3',5,5'-tetramethylbenzidine.

Detecting intact-VWF

Intact-VWF is referred as VWF being recognized by KB-VWF-D3.1. Briefly, wells coated with KB-VWF-D3.1 (5 μg/ml) were incubated with samples containing non-proteolyzed VWF, ADAMTS13-proteolyzed VWF or a mixture of both. Alternatively, plasma samples were used. Bound VWF was probed using polyclonal anti-VWF antibodies and detected via hydrolysis of 3,3',5,5'-tetramethylbenzidine.

Total VWF-antigen

Total VWF-antigen was measured in an elisa using polyclonal rabbit anti-VWF antibodies as described.[21]

Results

Selection of anti-VWF nanobodies

To isolate nanobodies that distinguish between intact or proteolyzed VWF, a selection method using rVWF and degraded-VWF was applied, generating 12 unique sequences (Figure 1A-C). Purified nanobodies were tested for interaction with rVWF and degraded-VWF. Whereas 10 of 12 nanobodies displayed similar binding to both VWF preparations, two of them were characterized by differential binding. First, rVWF associated in a dose-dependent manner to immobilized nanobody KB-VWF-D3.1, whereas binding of degraded-VWF to this nanobody was strongly reduced (Figure 1D). In these assays, pd-VWF yielded responses that were consistently lower than rVWF (93±4% compared to 100±2%; p=0.015; Figure 1E), probably due to degraded-VWF present in normal plasma. In complementary assays, KB-VWF-D3.1 bound 8-fold less efficiently to immobilized degraded-VWF compared to immobilized rVWF (Supplementary figure S1). As for KB-VWF-F1.1, efficient binding of degraded-VWF was detected, whereas binding of rVWF approached background levels (Figure 1F). Therefore, these two nanobodies were selected for further analysis.

Determination of the binding epitope for KB-VWF-F1.1

Since KB-VWF-F1.1 bound to degraded-VWF but not intact-VWF, we anticipated that this nanobody recognizes the region surrounding the Tyr^{1605}-Met^{1606} cleavage site. This was tested in an ADAMTS13-activity test utilizing its substrate FRETS-VWF73, which contains the VWF A2-domain sequence Asp^{1596}-Arg^{1668} (Supplemental figure S2A). Whereas KB-VWF-D3.1 and control nanobody KB-VWF-004 (against the region VWF/D4-CK) left substrate proteolysis unaffected, KB-VWF-F1.1 efficiently interfered with substrate conversion by ADAMTS13. This suggests that the epitope of VWF-KB-F1.1 is located within the region Asp^{1596}-Arg^{1668}. Of note, KB-VWF-F1.1 and MAB27642, which targets residues Arg^{1596}-Tyr^{1605}, did not compete for binding to degraded-VWF (Supplementary figure S2B), suggesting they recognize different epitopes within this region.

Determination of the binding epitope for KB-VWF-D3.1

To determine the epitope of KB-VWF-D3.1, we first analyzed binding of this nanobody to a series of rVWF fragments, *ie.* A1-Fc, A2-Fc, A3-Fc and D4-Fc. Surprisingly, KB-VWF-D3.1 bound most efficiently to the A3-Fc fragment rather than the A2-Fc (Figure 2A). Binding was similar when binding of fragments to immobilized KB-VWF-D3.1 was assessed (Supplementary figure S3A). Moreover, no binding of rVWF lacking the A3 domain to KB-VWF-D3.1 could be detected, whereas deletion of other domains left binding unaffected (Supplementary figure S3B).

To refine its binding site within the A3-domain, molecular modeling was performed (see supplementary materials). This procedure revealed that the top 30-ranked conformations of the complex all clustered similarly, with the nanobody docking onto 4 separate amino acid-stretches within the VWF A3-domain region Val^{1731}-Asn^{1818} (Figure 2B-D). Interestingly, 8 of the amino acids included in the epitope of KB-VWF-D3.1 have previously been recognized as being relevant for collagen binding (Figure 2E)[22], indicating that the epitope of KB-VWF-D3.1 overlaps the collagen binding site. Consequently, we compared the effect of KB-VWF-D3.1 to that of two known A3-domain binding antibodies (the C37h nanobody[23] and the Mab505 monoclonal antibody[24]) on binding of VWF to collagen type III. The positive controls C37h and Mab505 efficiently blocked pd-VWF-collagen interactions (Figure 2F). KB-VWF-D3.1 also dose-dependently reduced binding of pd-VWF to collagen, but less efficiently than antibodies C37h and Mab505 (Figure 2F). In addition, KB-VWF-D3.1 delayed VWF-dependent platelet-adhesion to collagen under flow-conditions (Supplementary figure S3C). Having their epitope overlapping the collagen binding site in common, it raises the question whether C37h and Mab505 can distinguish between intact and degraded-VWF akin to KB-VWF-D3.1. However, both C37h and Mab505 displayed similar binding to both intact rVWF and degraded-VWF (Figure 2G). Thus, nanobody KB-VWF-D3.1 is unique in binding to an epitope within the A3-domain, the exposure of which is modulated upon proteolysis within the A2-domain.

Effect multimer size on VWF binding to KB-VWF-D3.1

Proteolysis of VWF by ADAMTS13 results in loss of the Tyr^{1605}-Met^{1606} peptide bond, thereby reducing multimer size. We therefore tested how multimer size affects binding of VWF to immobilized KB-VWF-D3.1. First, we analyzed two distinct pd-VWF preparations that were obtained from pd-VWF concentrates via gel-filtration chromatography. One with HMW-multimers and one enriched in medium-sized molecular weight multimers (Figure 3A). Both fractions displayed similar binding to KB-VWF-D3.1 (Figure 3B). Next, we compared binding of dimeric rVWF/delta-pro to that of full-length rVWF (Figure 3C). Both dimeric rVWF/delta-pro and rVWF bound to KB-VWF-D3.1 with similar half-maximal binding (0.2±1 μg/ml vs 0.2±0.1 μg/ml; p=0.62). Apparently, binding of VWF to immobilized KB-VWF-D3.1 is independent of its multimer size. Reduced binding of degraded-VWF to KB-VWF-D3.1 is conceivably originating from proteolysis of the Tyr^{1605}-Met^{1606} peptide bond rather than from a reduction in multimer size.

Proteolysis of VWF over time

We next investigated the effect of ADAMTS13-proteolysis on VWF binding to KB-VWF-D3.1 and KB-VWF-F1.1 in a time-dependent manner. Briefly, pd-VWF was exposed to shear in the

presence of recombinant ADAMTS13 and samples were taken at indicated time-points (0-3h). Multimeric pattern and binding to both nanobodies were analyzed. Exposure to ADAMTS13 resulted in a time-dependent decrease in pd-VWF multimer size (Figure 4A). As expected, proteolysis was inhibited in the presence of EDTA, a metal-ion chelator which renders ADAMTS13 inactive. Concurrent with increased pd-VWF proteolysis, increased binding to KB-VWF-F1.1 was observed (Figure 4B). In contrast, binding of pd-VWF to KB-VWF-D3.1 disappeared in a complementary fashion (Figure 4B). These data validate that the binding of both nanobodies to VWF is dependent on the extent of proteolysis by ADAMTS13.

Measuring degraded-VWF in mixtures of intact and degraded-VWF

Given the specificity of both nanobodies for intact and degraded-VWF, respectively, we anticipated that they could be useful to determine the extent of VWF proteolysis in patient samples. In preliminary experiments, KB-VWF-F1.1 lacked sufficient sensitivity to detect minor proteolysis of VWF in plasma, and we therefore focused for the remainder of the study on KB-VWF-D3.1. We first analyzed to what extent increased proteolysis would be detectable. Different mixtures of purified rVWF and degraded-VWF were prepared, and the ratio intact VWF/total VWF-antigen was determined. A dose-dependent decrease of this ratio was observed, when the percentage of degraded-VWF in the samples increased (Figure 5A). From these experiments, it seems that an increase of approximately 10% degraded-VWF can be detected ($p=0.0009$ compared 100% intact).

Analysis of congenital VWD-patient plasma

We then analyzed plasma samples obtained from controls (n=31) and VWD-patients included in the French reference center for VWD (n=101).[19] The patient-cohort consisted of VWD-type 1 (n=20), VWD-type 2A (n=43), VWD-type 2B (n=24) and VWD-type 2M (n=14) patients.

To determine the amount of intact VWF, we calculated the amount of antigen obtained using KB-VWF-D3.1 (= intact-VWF) over the amount of total VWF-antigen, using normal pooled plasma as calibrator. By doing so, it appeared that the intact-VWF/total antigen ratio for controls was found to be 1.0±0.2 (Figure 5B). The ratio of intact-VWF/total VWF was decreased for each of the VWD-types analyzed. The ratio was 0.7±0.3 ($p=0.0004$) for VWD-type 1, 0.5±0.2 ($p<0.0001$) for VWD-type 2A, 0.6±0.2 ($p<0.0001$) for VWD-type 2B and 0.7±0.2 ($p=0.0148$) for VWD-type 2M (Figure 5B). A separate graph showing the ratio for each mutation is presented in the Supplementary figure S4. Since VWD-type 2A is divided in two subtypes, *ie.* VWD-type 2A-group 1 and VWD-type 2A-group 2, in which the loss of multimers is dominated by impaired multimerization and increased proteolysis, respectively, we separately analyzed samples from patients with VWD-type 2A-group 1 (n=14) and VWD-type

2A-group 2 (n=29). The ratio intact-VWF/total VWF-antigen was significantly lower in VWD-type 2A-group 2 (0.4±0.2) compared to VWD-type 2A-group 1 (0.6±0.2; p=0.0007; Figure 5C). Since it was unexpected to find a decreased ratio intact-VWF/total VWF-antigen in all VWD-types, we also verified whether this decreased ratio would correspond to a potential loss of HMW-multimers. Multimer analysis was available for a subset of samples, and we indeed observed that in all patient groups, including VWD-type 1 and type 2M, there was on average a relative decrease in the HMW-multimers (>10 multimer bands) compared to normal pooled plasma, (Figure 5D). An example of a multimeric pattern with reduced HMW-multimers for a VWD-type 1 and type 2M patient is provided in Supplementary figure S5. Interestingly, there was a significant correlation between the ratio intact-VWF/total VWF-antigen *versus* multimer size (r=0.51; p<0.0001; Figure 5E). Thus, it seems that in the majority of VWD-patients there is increased proteolysis compared to the normal population.

Analysis of AVWS-patient plasma

We next examined plasma from patients receiving ECMO-support (n=27) and from patients with severe aortic stenosis (n=17). Both patient groups are characterized by a loss of VWF HMW-multimers (Figure 6A), potentially caused by increased ADAMTS13-mediated proteolysis. Compared to normal control, the ratio of intact-VWF (measured by binding to KB-VWF-D3.1) over total VWF-antigen was significantly reduced for both patient groups: 0.85±0.09 (mean±SD; p=0.0017) and 0.78±0.13 (p<0.0001) for severe aortic stenosis and ECMO patients, respectively (Figure 6B). Of note, for both groups, there was a significant correlation between the ratio intact/total antigen and the presence of HMW-multimers (>10), with p-values being p=0.0463 for severe aortic stenosis-samples and p=0.0452 for ECMO-samples (Figures 6C-D). This may suggest that the loss of larger multimers indeed is predominantly due to proteolysis rather than other mechanisms.

Discussion

In this study, we describe a novel nanobody, designated KB-VWF-D3.1, that loses its capacity to bind VWF upon proteolysis by ADAMTS13. We show that this nanobody displays reduced binding to VWF present in plasma of congenital VWD patients as well in those having an acquired deficiency of VWF. Unexpectedly, this nanobody revealed the presence of increased VWF degradation in some patients with VWD-type 1 and 2M.

Structural conformational changes are key regulators of VWF function. Although there are several ways to monitor such structural changes, including functional assays and microscopic visualization, the use of specific antibodies is by far the most convenient and accessible approach. In 2005, a nanobody (AU-VWFa-11) was described that selectively binds to VWF in its active, glycoprotein Ibα-binding conformation, but not to globular inactive VWF.[25] This nanobody has indeed been useful to identify the presence of active VWF under several pathological conditions.[26-31] Following a similar strategy, we set out to identify nanobodies that distinguish between intact and ADAMTS13-proteolyzed VWF, leading to the successful identification of a nanobody that binds to intact- but not to degraded-VWF (Figure 1).

Admittedly, others have reported antibodies that distinguish intact- and degraded-VWF.[16,32] These antibodies have in common that they recognize the VWF A2-domain and only bind VWF in its elongated or proteolyzed conformation. Our nanobody is different from these antibodies in two distinct ways: first, it binds to VWF in both globular and elongated conformations (allowing it to detect intact-VWF in plasma samples), and second by having its epitope in the VWF A3-domain. Of course, binding to the A3-domain is perhaps less relevant from a diagnostic point of view, but its unique epitope may provide new insights into the structure-function relationship of VWF. Indeed, the identification of the epitope of KB-VWF-D3.1 being in the A3-domain was unexpected in the sense that proteolysis of VWF by ADAMTS13 takes place in the adjacent A2-domain. Nevertheless, a series of experiments undoubtedly led to the conclusion that KB-VWF-D3.1 indeed interacts with the A3-domain, and more specifically, that its epitope overlaps the collagen binding site (Figure 2; supplementary figure S3).

The notion that KB-VWF-D3.1 binds to the A3-domain clearly raises the question how proteolysis in the A2-domain may affect the exposure of the epitope of KB-VWF-D3.1 in the A3-domain? It has previously been shown that different domains within VWF can interact or communicate with each other. For instance, VWF has a 4-fold reduced affinity for FVIII when bound to collagen, suggesting that binding of the A3-domain to collagen affects the exposure of the FVIII binding site in the D'D3-region.[33] It is thus possible that proteolysis within the A2-domain may result in conformational changes in the A3-domain. Second, the D'D3-region and the A2-domain can both bind to the A1-domain.[34,35] From this perspective, the possibility exists that proteolysis in the A2-domain allows a portion of this domain to move towards the A3-

domain, binding to the adjacent epitope of KB-VWF-D3.1. Irrespective of the exact mechanism, given that this epitope overlaps the collagen binding site, it is tempting to speculate that there exists an additional mechanism by which ADAMTS13 reduces the hemostatic potential of VWF: not only would proteolysis reduce multimer size, but modulating the exposure of the collagen binding site could reduce the capacity of VWF to bind collagen. In this scenario, the ratio affected A3-domains/normal A3-domains would be determinant for the extent by which collagen binding is modulated. Additional experiments are warranted to explore this hypothesis in more detail.

Should the cleaved A2-domain indeed start covering the epitope of KB-VWF-D3.1, then this may also provide a possible explanation why KB-VWF-D3.1 but not the concurrent antibodies C37h and Mab505 distinguishes between intact and degraded VWF. Both antibodies have a significant higher affinity for VWF. As such, they would efficiently compete with the A2-domain for a common binding site within the A3-domain, and therefore be unable to detect proteolysis within the A2-domain.

Between both nanobodies KB-VWF-D3.1 and KB-VWF-F1.1, the former proved most sensitive in detecting degradation of VWF. Both monovalent and bivalent variants of KB-VWF-F1.1 did bind degraded VWF only at relatively high concentrations. In this respect, KB-VWF-F1.1 seems similar to the antibody described by Kato and coworkers.[16] It is possible that the low affinity originates from the flexible nature of their epitope, the polypeptides at either end of the Tyr^{1605}-Met^{1606} cleavage site.

Focusing on nanobody KB-VWF-D3.1, we investigated whether this nanobody could detect increased proteolysis in samples of patients. To do so, the nanobody should meet with a number of criteria: 1. binding should be independent of multimer size; 2. binding should decrease dose-dependently upon an increased presence of proteolyzed VWF; and 3. the nanobody should be sufficiently sensitive to detect low amounts of proteolyzed VWF. By performing a number of control experiments, it seems that KB-VWF-D3.1 indeed meets these three criteria (Fig. 3-5). In particular, the notion that the presence of 10% degraded-VWF could be detected is relevant.

Although this study has not been designed to validate the KB-VWF-D3.1-based assay as a diagnostic tool, we did analyze a series of control and patient samples. We measured both the amount of antigen detected using KB-VWF-D3.1 (referred to as intact-VWF) and the amount of antigen using polyclonal anti-VWF antibodies (referred to as total VWF-antigen). When analyzing 31 control samples from volunteers, the ratio intact-VWF/total VWF-antigen was 1.0±0.2 (mean±SD), with a 95% confidence interval being 0.9-1.1 (Figure 5). A few of these samples were either particularly low with a ratio <0.82 (mean-1xSD; 3 out of 31 samples) or particularly high (>1.20; mean+1xSD; 4/31 samples). Apparently, on average, the analyzed individual plasma samples do not contain less intact-VWF compared to the plasma calibrator.

However, there exists within this control group a number of individuals in which proteolysis of VWF seems somewhat up- or down-regulated.

We also had access to a large group of congenital VWD-patients. As expected, the intact-VWF/total VWF-antigen ratio was lowest in samples from VWD-type 2A-group 2 patients, who express mutated VWF that has increased sensitivity for ADAMTS13-mediated proteolysis.[12] Also for VWD-type 2B it has been reported that ADAMTS13 may contribute to the loss of larger multimers in these patients, but this degradation is very much mutation dependent.[13] Indeed, ratios between 0.14 and 1.03 were obtained in these samples, suggesting a high variability between VWD-type 2B patients. Unexpectedly, we also observed a decreased ratio intact-VWF/total VWF-antigen in part of patients with VWD-type 1 and VWD-type 2M, although to a lesser extent compared to VWD-type 2A and 2B. This suggests that there is an increase in VWF degradation in these samples compared to normal controls. If so, one would anticipate that there is a concordant loss of HMW-multimers. We indeed observed that compared to normal pooled plasma, all subtypes including VWD-type 1 and VWD-type 2M samples were characterized by reduced quantities of the larger multimers (Figure 5). Moreover, there was a highly significant correlation between the ratio intact VWF/total VWF-antigen and the presence of these larger multimers. It seems conceivable therefore that at least part of the loss of HMW-multimers can be explained by an increased degradation of VWF by ADAMTS13.

It is of interest to mention that we noticed quite some variation in the extent of VWF degradation in patients with a similar mutation (Supplementary figure S4). This suggests that besides the mutation itself, also other factors may contribute to the extent by which VWF is proteolyzed by VWF. One potential hypothesis could be that mutations allow VWF to unfold more easily during circulation, for instance at sites of bifurcations, making them more susceptible to proteolysis. This effect would be amplified if secondary conditions, like a developing atherosclerosis, further contribute to the presence of disturbed flow conditions. Whether this will be associated with a more pronounced bleeding phenotype remains to be investigated.

Excessive VWF degradation associated with a loss of HMW-multimers is also observed in AVWS, including in patients with severe aortic stenosis and ECMO-patients (Figure 6). It was perhaps unsurprising therefore that levels of intact-VWF were significantly reduced in both patient groups. As for the congenital VWD samples, both AVWS groups displayed a significant correlation between the ratio intact-VWF/total VWF-antigen and the presence of larger multimers. Importantly, the average loss of intact-VWF was less pronounced in severe aortic stenosis and ECMO-patients compared to congenital VWD-patients.

We noted that degradation of VWF was more pronounced in VWD-type 2A-group 2 patients and *in vitro* degradation-assays compared to AVWS patients, although all are exposed to conditions that favor VWF degradation. This difference can be explained by the fact that VWF

is constitutively in a ADAMTS13-sensitive conformation in VWD-type 2A-group 2 and in the *in vitro* degradation assays, allowing both large and short multimers to be proteolyzed. In contrast, in AVWS, VWF is elongated during a short period of time, when passing the stenosed valve or the mechanic pump. Such conditions particularly favor proteolysis of the larger multimers only, with the highest chances of cleavage occurring within the middle region of these multimers (Supplementary figure S6).

Taken together, we have developed a novel nanobody that binds to the A3-domain of VWF, a subunit that is not proteolyzed by ADAMTS13. This nanobody not only provided new insight into how ADAMTS13 may regulate the exposure of the collagen binding site within the A3-domain, but it also identified the presence of low-grade VWF degradation in a large amount of patient samples. By using its sensitivity, we revealed an increase in VWF degradation in VWD-type 1 and 2M samples, which we were unable to do with assays currently available for detecting degraded-VWF.

Whether KB-VWF-D3.1 could be useful as a diagnostic tool regarding congenital VWD would need to be established in additional studies designed for this specific purpose. However, we anticipate that our assay might be useful in a number of other situations. First, we now that in the majority of aortic stenosis patients that undergo transcatheter valve replacement, the VWF degradation defect is corrected within 5-10 minutes after valve placement.[11,36] However, the VWF degradation defect is not corrected in 10-20% of the patients due to incorrect valve placement that causes regurgitation. Currently, no point-of-care assays are available to verify the correct placement of the valves. It is possible that a point-of-care assay using KB-VWF-D3.1 could be applied for this purpose, as it will detect an increase in levels of intact-VWF. Second, this rapid point-of-care approach can also be used to test the opposite, *ie.* if there is loss of VWF degradation due to a lack of ADAMTS13 activity. This could eventually facilitate the clinical decision-making of patients that arrive into the hospital with suspected thrombotic thrombocytopenic purpura.

Funding: This study received funding from the National Research Agency (Agence Nationale de la Recherche, grant numbers ANR-17-RHUS-17-0011-WIIIAssistHeart and ANR-21-CE14-0076-02-Vista) and the foundation Crédit Agricole Nord de France.

Acknowledgements: The authors thank Drs. Jenny Goudemand, Edith Fressinaud, Mouhamed Moussa, Christophe Zawadzki and Pierre Boisseau for the development, patient recruitment and genetic analysis of the patient cohort in the framework of the CRMW.

Conflict of interest: GLF, SL, SD and TD are employees of Diagnostica Stago. The other authors declare no conflict of interest.

References

1. Springer TA. von Willebrand factor, Jedi knight of the bloodstream. *Blood.* 2014;124(9):1412-1425.
2. Lenting PJ, Christophe OD, Denis CV. von Willebrand factor biosynthesis, secretion, and clearance: connecting the far ends. *Blood.* 2015;125(13):2019-2028.
3. Levy GG, Nichols WC, Lian EC, et al. Mutations in a member of the ADAMTS gene family cause thrombotic thrombocytopenic purpura. *Nature.* 2001;413(6855):488-494.
4. Crawley JT, de Groot R, Xiang Y, Luken BM, Lane DA. Unraveling the scissile bond: how ADAMTS13 recognizes and cleaves von Willebrand factor. *Blood.* 2011;118(12):3212-3221.
5. Dong JF, Moake JL, Nolasco L, et al. ADAMTS-13 rapidly cleaves newly secreted ultralarge von Willebrand factor multimers on the endothelial surface under flowing conditions. *Blood.* 2002;100(12):4033-4039.
6. De Ceunynck K, De Meyer SF, Vanhoorelbeke K. Unwinding the von Willebrand factor strings puzzle. *Blood.* 2013;121(2):270-277.
7. De Ceunynck K, Rocha S, Feys HB, et al. Local elongation of endothelial cell-anchored von Willebrand factor strings precedes ADAMTS13 protein-mediated proteolysis. *J Biol Chem.* 2011;286(42):36361-36367.
8. Springer TA. Biology and physics of von Willebrand factor concatamers. *J Thromb Haemost.* 2011;9 Suppl 1:130-143.
9. Vincentelli A, Susen S, Le Tourneau T, et al. Acquired von Willebrand syndrome in aortic stenosis. *N Engl J Med.* 2003;349(4):343-349.
10. Van Belle E, Rauch A, Vincentelli A, et al. Von Willebrand factor as a biological sensor of blood flow to monitor percutaneous aortic valve interventions. *Circ Res.* 2015;116(7):1193-1201.
11. Vincent F, Rauch A, Loobuyck V, et al. Arterial Pulsatility and Circulating von Willebrand Factor in Patients on Mechanical Circulatory Support. *J Am Coll Cardiol.* 2018;71(19):2106-2118.
12. Haberichter SL, Fahs SA, Montgomery RR. von Willebrand factor storage and multimerization: 2 independent intracellular processes. *Blood.* 2000;96(5):1808-1815.
13. Rayes J, Hommais A, Legendre P, et al. Effect of von Willebrand disease type 2B and type 2M mutations on the susceptibility of von Willebrand factor to ADAMTS-13. *J Thromb Haemost.* 2007;5(2):321-328.
14. Budde U. Diagnosis of von Willebrand disease subtypes: implications for treatment. *Haemophilia.* 2008;14 Suppl 5:27-38.
15. Sharma R, Flood VH. Advances in the diagnosis and treatment of Von Willebrand disease. *Blood.* 2017;130(22):2386-2391.

16. Kato S, Matsumoto M, Matsuyama T, Isonishi A, Hiura H, Fujimura Y. Novel monoclonal antibody-based enzyme immunoassay for determining plasma levels of ADAMTS13 activity. *Transfusion.* 2006;46(8):1444-1452.
17. Rauch A, Caron C, Vincent F, et al. A novel ELISA-based diagnosis of acquired von Willebrand disease with increased VWF proteolysis. *Thromb Haemost.* 2016;115(5):950-959.
18. Kubo M, Sakai K, Hayakawa M, et al. Increased cleavage of von Willebrand factor by ADAMTS13 may contribute strongly to acquired von Willebrand syndrome development in patients with essential thrombocythemia. *J Thromb Haemost.* 2022.
19. Veyradier A, Boisseau P, Fressinaud E, et al. A Laboratory Phenotype/Genotype Correlation of 1167 French Patients From 670 Families With von Willebrand Disease: A New Epidemiologic Picture. *Medicine (Baltimore).* 2016;95(11):e3038.
20. Moutel S, Bery N, Bernard V, et al. NaLi-H1: A universal synthetic library of humanized nanobodies providing highly functional antibodies and intrabodies. *Elife.* 2016;5:e16228.
21. Lenting PJ, Westein E, Terraube V, et al. An experimental model to study the in vivo survival of von Willebrand factor. Basic aspects and application to the R1205H mutation. *J Biol Chem.* 2004;279(13):12102-12109.
22. Romijn RA, Westein E, Bouma B, et al. Mapping the collagen-binding site in the von Willebrand factor-A3 domain. *J Biol Chem.* 2003;278(17):15035-15039.
23. Wohner N, Sebastian S, Muczynski V, et al. Osteoprotegerin modulates platelet adhesion to von Willebrand factor during release from endothelial cells. *J Thromb Haemost.* 2022;20(3):755-766.
24. Navarrete AM, Casari C, Legendre P, et al. A murine model to characterize the antithrombotic effect of molecules targeting human von Willebrand factor. *Blood.* 2012;120(13):2723-2732.
25. Hulstein JJ, de Groot PG, Silence K, Veyradier A, Fijnheer R, Lenting PJ. A novel nanobody that detects the gain-of-function phenotype of von Willebrand factor in ADAMTS13 deficiency and von Willebrand disease type 2B. *Blood.* 2005;106(9):3035-3042.
26. Groot E, de Groot PG, Fijnheer R, Lenting PJ. The presence of active von Willebrand factor under various pathological conditions. *Curr Opin Hematol.* 2007;14(3):284-289.
27. Djamiatun K, van der Ven AJ, de Groot PG, et al. Severe dengue is associated with consumption of von Willebrand factor and its cleaving enzyme ADAMTS-13. *PLoS Negl Trop Dis.* 2012;6(5):e1628.
28. Hyseni A, Kemperman H, de Lange DW, Kesecioglu J, de Groot PG, Roest M. Active von Willebrand factor predicts 28-day mortality in patients with systemic inflammatory response syndrome. *Blood.* 2014;123(14):2153-2156.

29. Chen J, Hobbs WE, Le J, Lenting PJ, de Groot PG, Lopez JA. The rate of hemolysis in sickle cell disease correlates with the quantity of active von Willebrand factor in the plasma. *Blood.* 2011;117(13):3680-3683.
30. Rutten B, Maseri A, Cianflone D, et al. Plasma levels of active Von Willebrand factor are increased in patients with first ST-segment elevation myocardial infarction: a multicenter and multiethnic study. *Eur Heart J Acute Cardiovasc Care.* 2015;4(1):64-74.
31. Chen SF, Xia ZL, Han JJ, et al. Increased active von Willebrand factor during disease development in the aging diabetic patient population. *Age (Dordr).* 2013;35(1):171-177.
32. Zhang L, Su J, Shen F, et al. A novel monoclonal antibody against the von Willebrand Factor A2 domain reduces its cleavage by ADAMTS13. *J Hematol Oncol.* 2017;10(1):42.
33. Bendetowicz AV, Wise RJ, Gilbert GE. Collagen-bound von Willebrand factor has reduced affinity for factor VIII. *J Biol Chem.* 1999;274(18):12300-12307.
34. Ulrichts H, Udvardy M, Lenting PJ, et al. Shielding of the A1 domain by the D'D3 domains of von Willebrand factor modulates its interaction with platelet glycoprotein Ib-IX-V. *J Biol Chem.* 2006;281(8):4699-4707.
35. Martin C, Morales LD, Cruz MA. Purified A2 domain of von Willebrand factor binds to the active conformation of von Willebrand factor and blocks the interaction with platelet glycoprotein Ibalpha. *J Thromb Haemost.* 2007;5(7):1363-1370.
36. Van Belle E, Rauch A, Vincent F, et al. Von Willebrand Factor Multimers during Transcatheter Aortic-Valve Replacement. *N Engl J Med.* 2016;375(4):335-344.

Legends

Figure 1: Generation of anti-VWF nanobodies.

A: Flow-diagram of screening approach using recombinant VWF (rVWF) and degraded-VWF for the isolation of anti-VWF nanobodies that distinguish between intact and degraded-VWF. ***B:*** SDS-Agarose gel (2%) of rVWF (lane 1) and the degraded-VWF preparation (lane 2) used for screening. ***C:*** Coomassie-staining of an SDS-Page gel under reducing conditions containing the degraded-VWF preparation used for screening. Arrows indicate intact VWF (a) and degraded-VWF fragments (b & c), respectively. ***D-F:*** Dose-response of rVWF (black circles) and degraded-VWF (grey circles) to immobilized nanobody KB-VWF-D3.1 (5 μg/ml; panel D) or KB-VWF-F1.1 (5 μg/ml; panel F). Panel E compares rVWF to plasma-derived VWF (pdVWF), both added at a concentration of 5 μg/ml. Bound VWF was probed using peroxidase-labeled polyclonal anti-VWF antibodies and detected via hydrolysis of 3,3',5,5'-tetramethylbenzidine. Data represent mean±SD of 4-8 experiments.

Figure 2: KB-VWF-D3.1 binds to the VWF A3-domain.

A: Binding of KB-VWF-D3.1 (1 μg/ml) to various concentrations of VWF domain-Fc fusion proteins (0-10 nM) that were captured onto anti-human Fc antibodies. Bound KB-VWF-D3.1 was probed using peroxidase-labeled polyclonal rabbit anti-cMyc antibodies and detected following hydrolysis of 3,3',5,5'-tetramethylbenzidine. A1-Fc: grey squares; A2-Fc: black triangles; A3-Fc: black circles; D4-Fc: white circles. Data represent mean±SD of 3 experiments. ***B:*** *In silico* simulation of KB-VWF-D3.1 (colored structures) docking on the VWF A3-domain (grey structure). Shown are the top 30-ranked structures of KB-VWF-D3.1, which all bind in a similar fashion to the A3-domain. ***C:*** Single structure representation of KB-VWF-D3.1 binding to the A3-domain. ***D:*** The VWF A3-domain, with residues in red representing amino acids predicted to be in the epitope of KB-VWF-D3.1. Residues known to affect collagen binding are indicated in yellow. ***E:*** Amino acid sequence of the VWF A3-domain, with the residues predicted to harbor the epitope for KB-VWF-D3.1 in red. Residues previously reported to be involved in collagen binding[22] are boxed. ***F:*** Inhibition of pd-VWF binding to collagen-type III by KB-VWF-D3.1 (closed circles), monoclonal antibody Mab505 (grey squares) and nanobody C37h (open circles). Presented is residual pd-VWF binding *versus* nanobody/antibody concentration. Data represent mean±SD of three experiments. ***G:*** Binding of pd-VWF (closed symbols) or degraded-VWF (open symbols) to immobilized Mab505 (5 μg/ml; circles) or C37h (5 μg/ml; squares). Bound pd-VWF was probed using peroxidase-labeled polyclonal anti-VWF antibodies and detected via hydrolysis of 3,3',5,5'-tetramethylbenzidine. Data represent mean±SD of 3 experiments.

Figure 3: Binding of VWF with varying multimer size to KB-VWF-D3.1

A: pd-VWF concentrates were applied to gel-filtration chromatography using Bio-Gel-A-15m. Fractions enriched in high molecular weight-multimers (HMW-VWF) and medium molecular weight-multimers (MMW-VWF) were analyzed for their multimeric pattern using SDS-agarose (2%) electrophoresis. ***B:*** Binding of HMW-VWF (closed circles) and MMW-VWF (open circles) to immobilized KB-VWF-D3.1 (5 μg/ml). ***C.*** Binding of multimeric rVWF (closed circles) and the dimeric VWF/delta-pro variant (grey squares) to immobilized KB-VWF-D3.1 (5 μg/ml). In both panels, bound VWF was probed using peroxidase-labeled polyclonal anti-VWF antibodies and detected via hydrolysis of 3,3',5,5'-tetramethylbenzidine. Data represent mean±SD of 3-4 independent measurements.

Figure 4: ADAMTS13-mediated proteolysis modulates binding of VWF to KB-VWF-D3.1 and KB-VWF-F1.1.

A: Purified pd-VWF was incubated with recombinant ADAMTS13 and exposed to vortex-induced shear. Samples taken at indicated time-points (0-3h) were analyzed via SDS-agarose electrophoresis. As a control, pd-VWF was exposed to ADAMTS13 and shear for 3 h in the presence of EDTA, a chelating agent that blocks ADAMTS13 activity. ***B:*** Samples were analyzed for total VWF-antigen using polyclonal antibodies, for the presence of intact-VWF using KB-VWF-D3.1 and for the presence of degraded-VWF using KB-VWF-F1.1. Presented is the ratio intact-VWF/total VWF-antigen (closed circles; left Y-axis) and the ratio degraded-VWF/total VWF-antigen (grey squares; right Y-axis) versus exposure time to ADAMTS13. Normal pooled plasma was used as calibrator for KB-VWF-D3.1, whereas a degraded-VWF preparation was used as calibrator for KB-VWF-F1.1. Data represent mean±SD of 3 independent experiments.

Figure 5: Detection of intact VWF in congenital VWD

A: VWF-deficient plasma was spiked with different amounts of purified rVWF and degraded-VWF, and incubated in microtiter plates coated with KB-VWF-D3.1. Bound VWF was probed using peroxidase-labeled polyclonal anti-VWF antibodies and detected via hydrolysis of 3,3',5,5'-tetramethylbenzidine. Data represent mean±SD of 3-4 independent measurements. The solid line illustrates the best linear fit, with 95% confidence interval indicated with the dotted lines. The vertical line indicates 90% intact rVWF supplemented with 10% degraded-VWF ***B-C:*** Patient plasma samples were analyzed for total antigen using polyclonal antibodies and for intact-VWF using KB-VWF-D3.1. Normal pooled plasma was used as calibrator. Presented is the ratio intact-VWF/total VWF-antigen. Each individual sample is represented

by a closed symbol. Statistical analysis was performed via a one-way Anova with Dunnett's correction for multiple comparisons (*panel B*) or Mann-Whitney (*panel C*). ***D:*** Multimers were analyzed via SDS-agarose electrophoresis. The relative amount of multimers exceeding 10 bands was determined via comparison to normal pooled plasma (NPP). ***E:*** Plotted is the ratio intact-VWF/total VWF-antigen *versus* the relative amount of large multimers. Correlation was determined in using Graphpad Prism Software.

Figure 6: Detection of intact VWF in AVWS

A: Multimers were analyzed via SDS-agarose electrophoresis. The relative amount of multimers exceeding 10 bands was determined via comparison to normal pooled plasma (NPP). ***B:*** Patient plasma samples were analyzed for total antigen using polyclonal antibodies and for intact-VWF using KB-VWF-D3.1. Normal pooled plasma was used as calibrator. Presented is the ratio intact-VWF/total VWF-antigen. Each individual sample is represented by a closed symbol. Statistical analysis was performed via a one-way Anova with Dunnett's correction for multiple comparisons. Control samples were identical to those presented in Figure 5. ***C-D:*** Plotted is the ratio intact-VWF/total VWF-antigen *versus* the relative amount of large multimers for samples from patients with severe aortic stenosis (AS; *panel C*) and from ECMO patients (*panel D*).

Figure 1

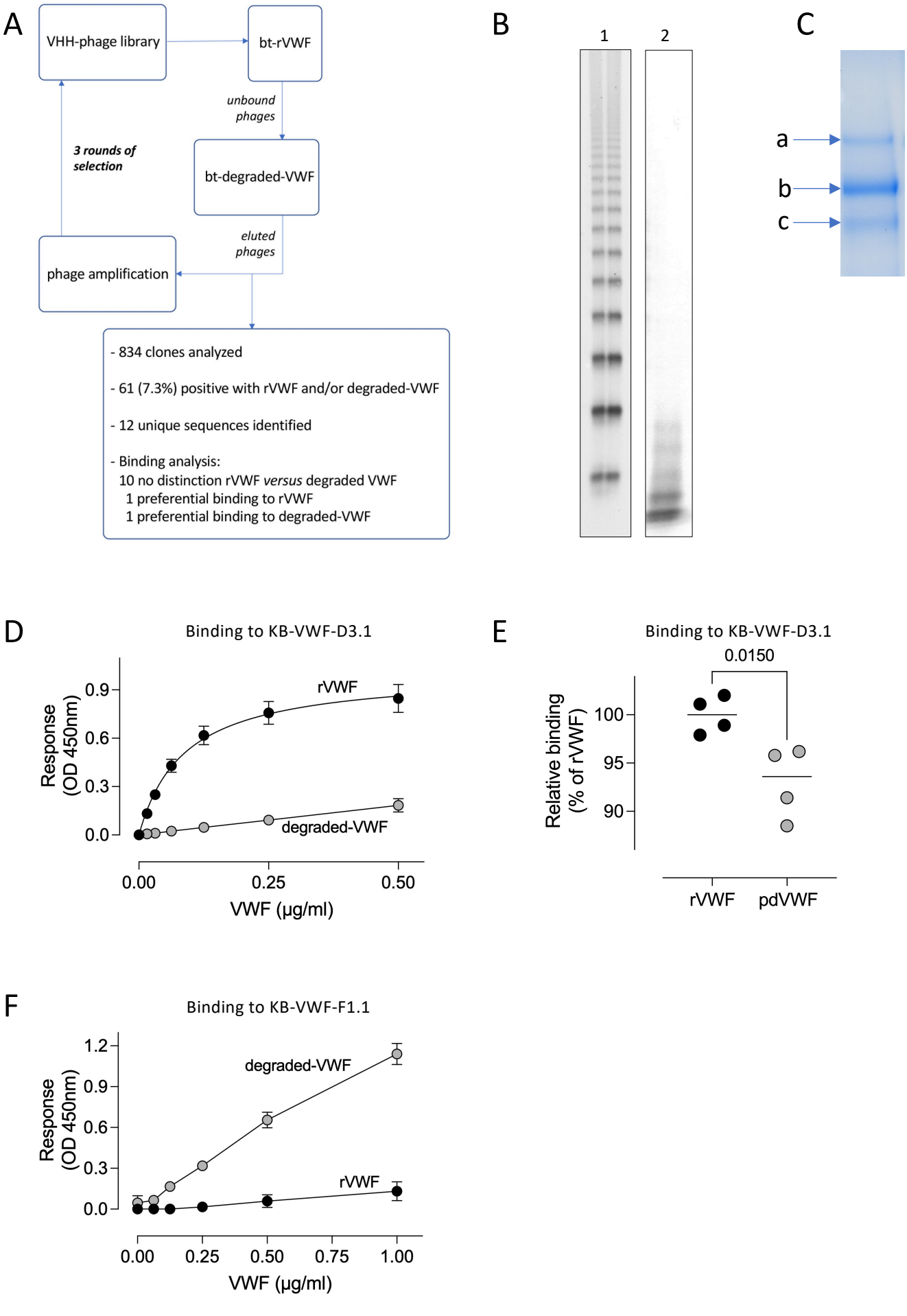
A
VHH-phage library
bt-rVWF
unbound phages
3 rounds of selection
bt-degraded-VWF
eluted phages
phage amplification
- 834 clones analyzed
- 61 (7.3%) positive with rVWF and/or degraded-VWF
- 12 unique sequences identified
- Binding analysis:
10 no distinction rVWF versus degraded VWF
1 preferential binding to rVWF
1 preferential binding to degraded-VWF
B
1
2
C
a
b
c
D
Binding to KB-VWF-D3.1
Response (OD 450nm)
0.0
0.3
0.6
0.9
rVWF
degraded-VWF
0.00
0.25
0.50
VWF (µg/ml)
E
Binding to KB-VWF-D3.1
0.0150
Relative binding (% of rVWF)
90
95
100
rVWF
pdVWF
F
Binding to KB-VWF-F1.1
Response (OD 450nm)
0.0
0.3
0.6
0.9
1.2
degraded-VWF
rVWF
0.00
0.25
0.50
0.75
1.00
VWF (µg/ml)

Figure 2

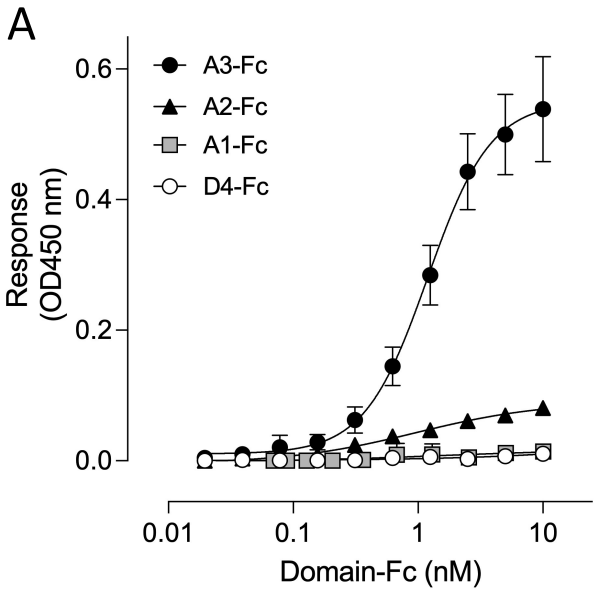
A
A3-Fc
A2-Fc
A1-Fc
D4-Fc
Response (OD450 nm)
0.6
0.4
0.2
0.0
0.01
0.1
1
10
Domain-Fc (nM)

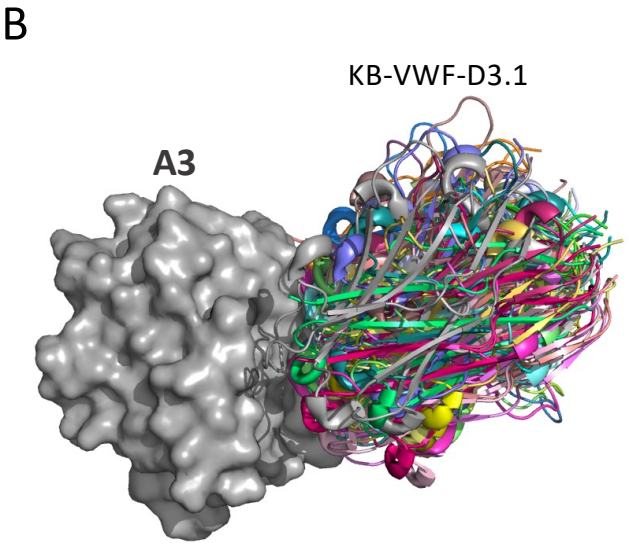
B
KB-VWF-D3.1
A3

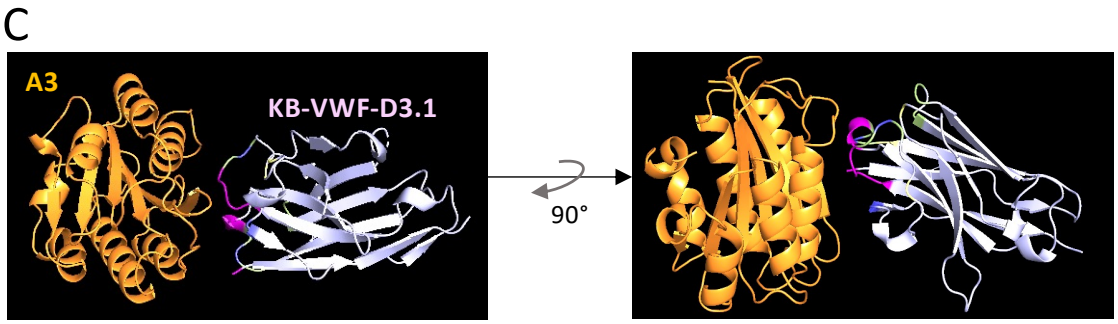
C
A3
KB-VWF-D3.1
90°


D


E
1688-Q P L D V I L L L D G S S S F P A S
Y F D E M K S F A K A F I S K A N I
G P R L T Q V S V L Q Y G S I T T I
D V P W N V V P E K A H L L S L V D
V M Q R E G G P S Q I G D A L G F A
V R Y L T S E M H G A R P G A S K A
V V I L V T D V S V D S V D A A A D
A A R S N R V T V F P I G I G D R Y
D A A Q L R I L A G P A G D S N V V
K L Q R I E D L P T M V T L G N S F-1867

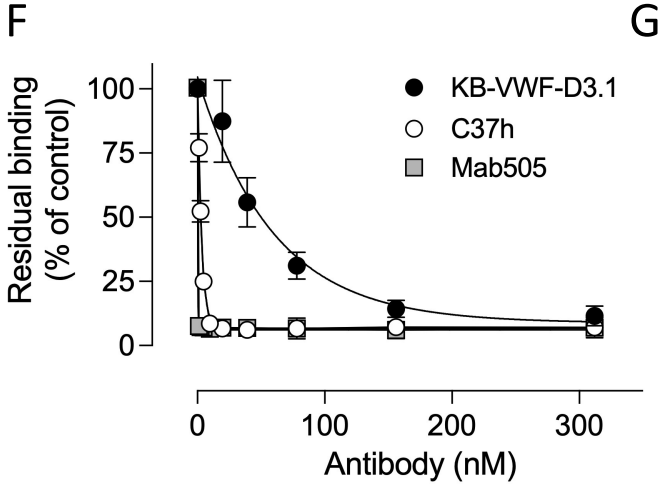
F
Residual binding (% of control)
100
75
50
25
0
KB-VWF-D3.1
C37h
Mab505
0
100
200
300
Antibody (nM)

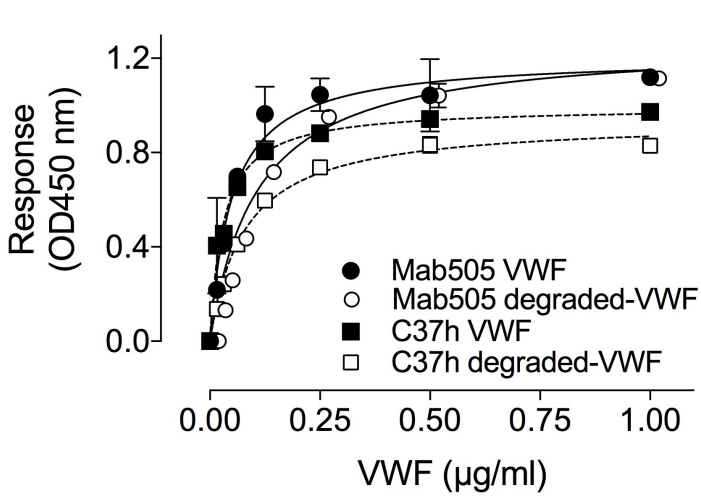
G
Response (OD450 nm)
1.2
0.8
0.4
0.0
Mab505 VWF
Mab505 degraded-VWF
C37h VWF
C37h degraded-VWF
0.00
0.25
0.50
0.75
1.00
VWF (µg/ml)

Figure 3

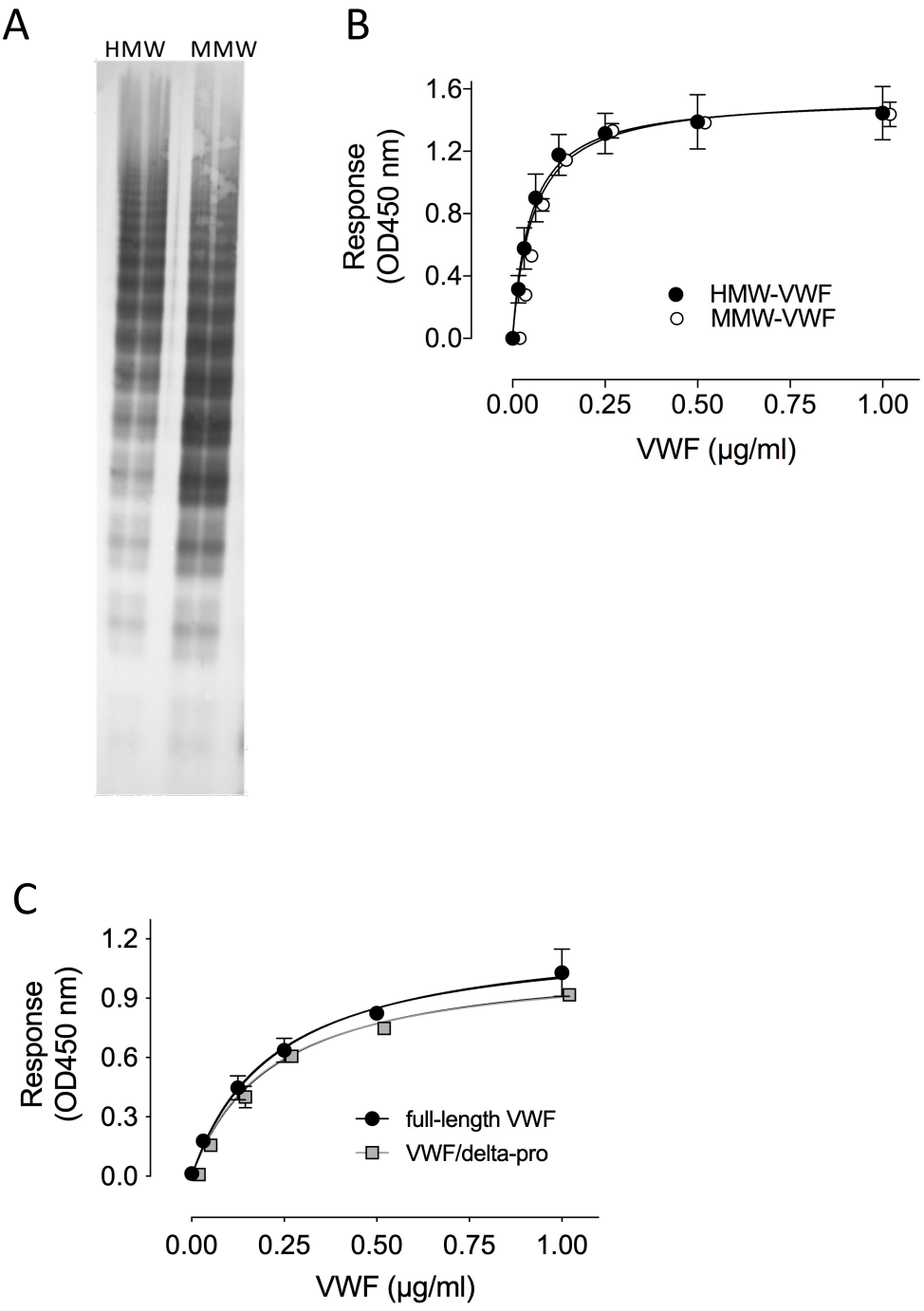
A
HMW
MMW
B
Response (OD450 nm)
1.6
1.2
0.8
0.4
0.0
HMW-VWF
MMW-VWF
0.00
0.25
0.50
0.75
1.00
VWF (µg/ml)
C
Response (OD450 nm)
1.2
0.9
0.6
0.3
0.0
full-length VWF
VWF/delta-pro
0.00
0.25
0.50
0.75
1.00
VWF (µg/ml)

Figure 4

A

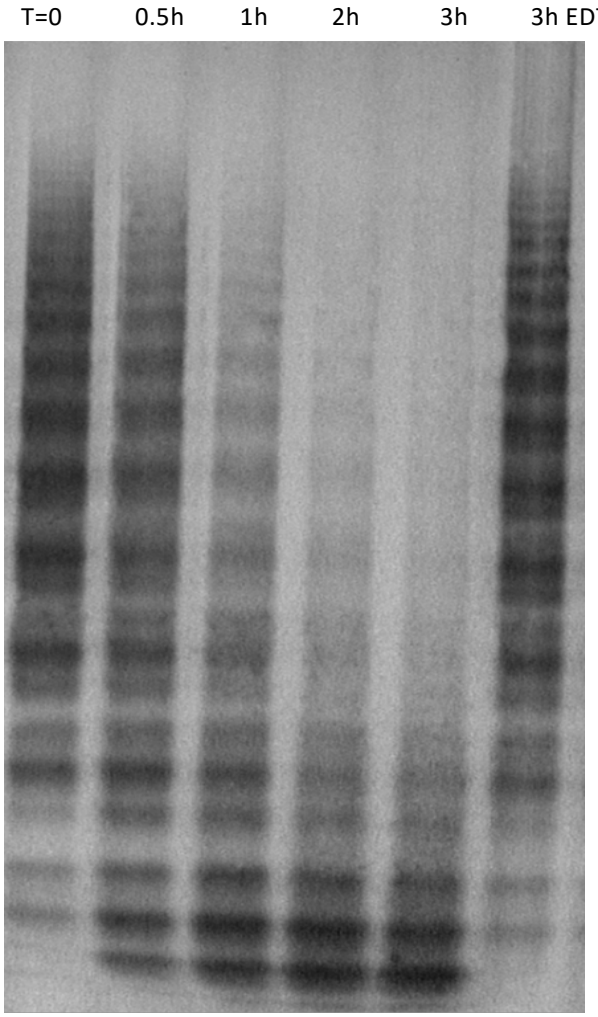
T=0
0.5h
1h
2h
3h
3h EDTA

B

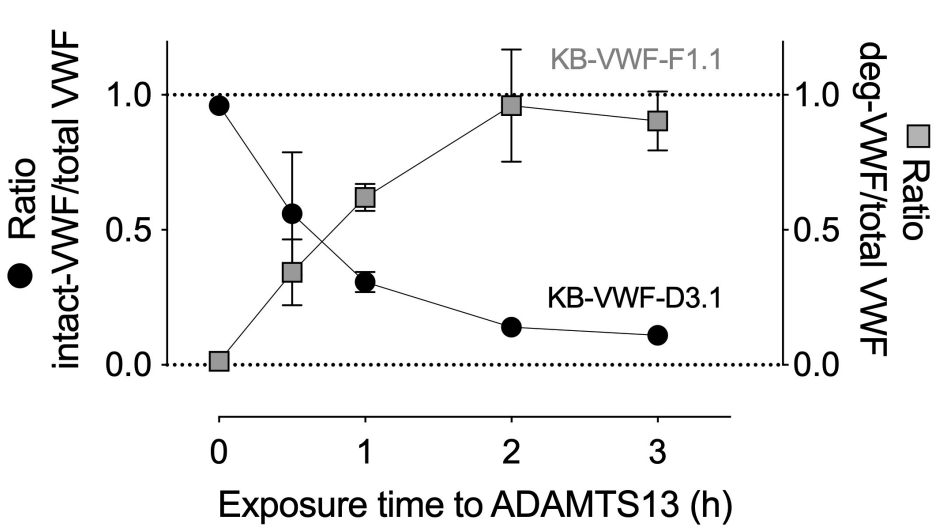
KB-VWF-F1.1
KB-VWF-D3.1
Ratio
intact-VWF/total VWF
Ratio
deg-VWF/total VWF
1.0
0.5
0.0
1.0
0.5
0.0
0
1
2
3
Exposure time to ADAMTS13 (h)

Figure 5

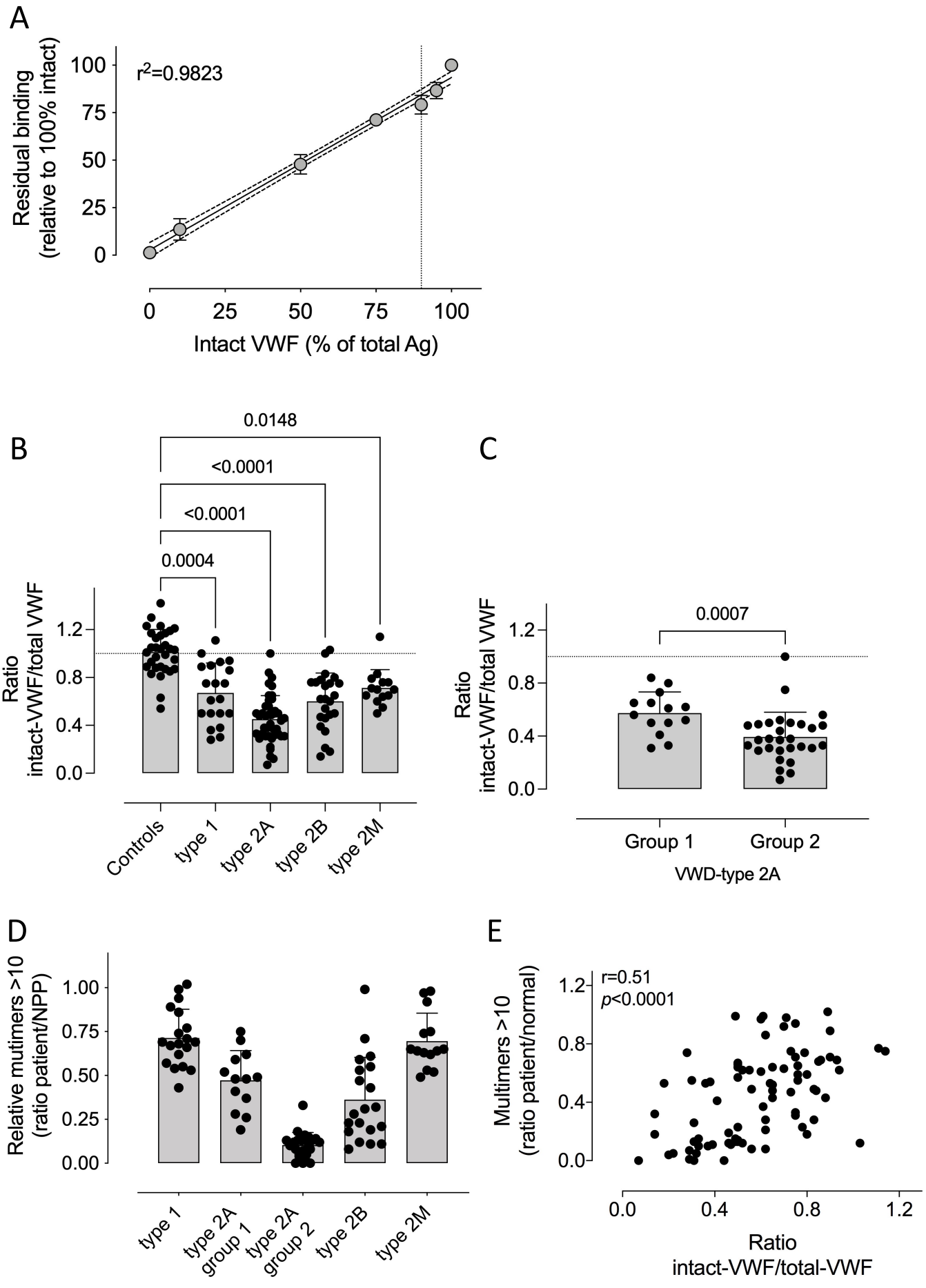
A
Residual binding (relative to 100% intact)
r²=0.9823
Intact VWF (% of total Ag)
B
Ratio intact-VWF/total VWF
0.0148
<0.0001
<0.0001
0.0004
Controls
type 1
type 2A
type 2B
type 2M
C
Ratio intact-VWF/total VWF
0.0007
Group 1
Group 2
VWD-type 2A
D
Relative mutimers >10 (ratio patient/NPP)
type 1
type 2A group 1
type 2A group 2
type 2B
type 2M
E
Multimers >10 (ratio patient/normal)
r=0.51
p<0.0001
Ratio intact-VWF/total-VWF

Figure 6

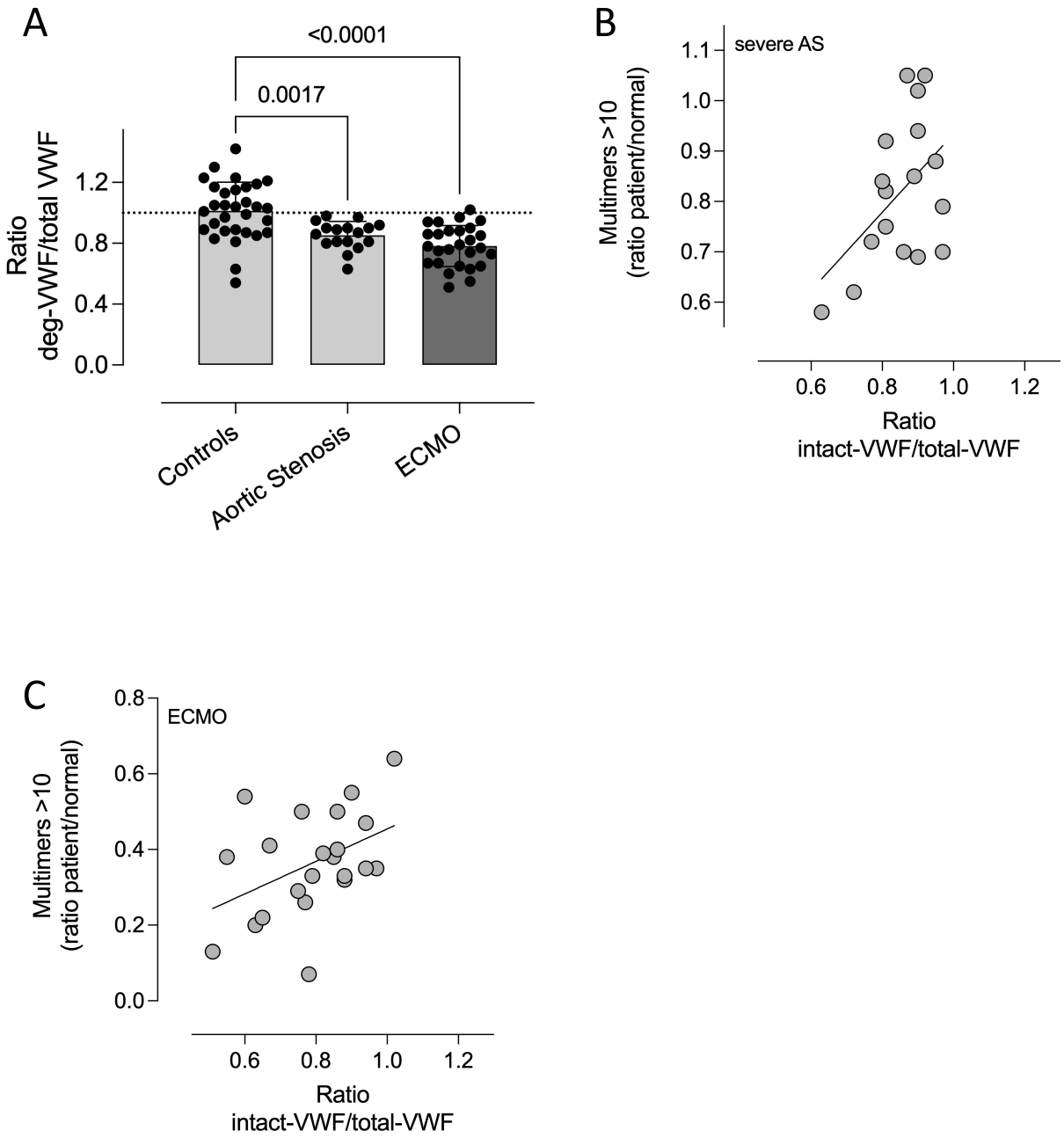
A
<0.0001
0.0017
Ratio
deg-VWF/total VWF
1.2
0.8
0.4
0.0
Controls
Aortic Stenosis
ECMO
B
severe AS
Multimers >10
(ratio patient/normal)
1.1
1.0
0.9
0.8
0.7
0.6
0.6
0.8
1.0
1.2
Ratio
intact-VWF/total-VWF
C
ECMO
Multimers >10
(ratio patient/normal)
0.8
0.6
0.4
0.2
0.0
0.6
0.8
1.0
1.2
Ratio
intact-VWF/total-VWF